Significantly fast spinodal decomposition and inhomogeneous nanoscale martensitic transformation in Ti–Nb–O alloys

Yuya ISHIGURO*[1], Yuhki TSUKADA[1], Toshiyuki KOYAMA[1]

[1] Department of Materials Design Innovation Engineering, Graduate School of Engineering, Nagoya University, Furo-cho, Chikusa-ku, Nagoya 464-8603, Japan

*Corresponding author (first author): Tel.: +81-52-789-3613, E-mail address: ishiguro.yuya@e.mbox.nagoya-u.ac.jp

The β phase spinodal decomposition during continuous cooling in Ti−Nb−O alloys is investigated by the phase-field method. Addition of only a few at.%O to Ti−23Nb (at.%) alloy remarkably increases the driving force of the β phase spinodal decomposition. During isothermal heat treatment at 1000 K and 1100 K in Ti−23Nb−3O (at.%) alloy, the β phase separates into β_1 phase denoted as $(Ti)_1(O, Va)_3$ and β_2 phase denoted as $(Ti, Nb)_1(Va)_3$, resulting in the formation of nanoscale concentration modulation. The phase decomposition progresses in 0.3−20 ms. In Ti−23Nb−*X*O alloys (*X* = 1.0, 1.2, 2.0), the spinodal decomposition occurs during continuous cooling with the rate of 500 K s^{-1}, indicating that the spinodal decomposition occurs during water quenching in the alloys. It is assumed that there is a threshold value of oxygen composition for inducing the spinodal decomposition because it does not occur during continuous cooling in Ti−23Nb−0.6O (at.%) alloy. The concentration modulation introduced by the β phase decomposition has significant effect on the β→α" martensitic transformation. Hence, it seems that for controlling microstructure and mechanical properties of Ti−Nb−O alloys, careful control of heat treatment temperature and cooling rate condition is required.

1. Introduction

Some β-type Ti−Nb alloys have shape-memory and superelasticity properties and are applied to biomedical materials [1-3]. The shape-memory and superelasticity properties of the alloys are derived from the martensitic transformation (MT) from the β phase (with a body-centered cubic lattice) to the α" phase (with a face-centered orthorhombic lattice). Miyazaki *et al.* have reported that in oxygen added Ti−Nb alloys, the long-range MT is suppressed and the nanoscale lattice-modulated domain is formed instead, which is called nanodomain [4-8]. In general, the oxygen is known as a typical α-stabilizing element and its addition to Ti-based alloys is assumed to promote the MT from the β phase to the α" phase (or α' phase with a hexagonal lattice). Hence, effects of the oxygen addition on the MT and the nanodomain formation have long been unclear [6,7,9].

In a previous phase-field simulation study, we proposed that the nanodomain formation can be explained by the diffusional-displacive transformation [10]. The oxygen addition to a Ti−Nb alloy promotes the nanoscale spinodal decomposition of the β phase into Nb-lean β_1 phase and Nb-rich β_2 phase at 1073 K or 1173 K, which are typical homogenization temperatures of Ti−Nb-based alloys. Because of the difference of Nb concentration between the β_1 and β_2 phases, the selective β_1→α" MT occurs at 300 K, resulting in the nanodomain formation.

The phase separation occurs in Ti−Ta [11], Ti−Mo [12] and Ti−Nb alloys [13]. In Ti−Nb binary system, the β phase separation region does not exist in the equilibrium phase diagram but it appears in the metastable phase diagram considering only the β and ω phases [14]. The spinodal decomposition in Ti−Nb-based alloys has been observed experimentally in a Ti−Nb−Ta−Zr alloy via three-dimensional atom-probe tomography [15,16]. It has been suggested that the MT behavior and mechanical properties of the alloy can be influenced by the concentration modulation of Ti and Nb introduced by the spinodal decomposition [17]. Therefore, the precise knowledge about the β phase spinodal decomposition in Ti−Nb-based alloys is necessary to control the mechanical properties of the alloys.

In this study, the β phase spinodal decomposition in Ti−Nb−O alloys during water quenching is investigated by the phase-field method. In the calculation of the total free energy of the system, the Gibbs energy and the gradient energy are considered. The Gibbs energy is formulated based on the CALPHAD method [18] and the thermodynamic parameters of the phase diagram of the Ti−Nb−O system are used. In order to discuss the time scale of the simulation quantitatively, the diffusion mobility is related to the experimental data on the diffusion coefficients of Nb and O in β-type Ti-based alloys.

2. Calculation method

The field variable $z_X(\mathbf{r},t)$ is defined using the mole fraction $x_X(\mathbf{r},t)$ as follows [19]:

$$z_X(\mathbf{r},t) = \frac{x_X(\mathbf{r},t)}{1 - x_{\mathrm{O}}(\mathbf{r},t)}, \quad (X = \mathrm{Ti}, \mathrm{Nb}, \mathrm{O}), \tag{1}$$

where *X* denotes the components (*X* = Ti, Nb, O), and **r** and *t* denote positional vector and time, respectively. The $z_{\mathrm{Nb}}(\mathbf{r},t)$ and $z_{\mathrm{O}}(\mathbf{r},t)$ are regarded as independent variables, and their temporal evolution is calculated by the Cahn−Hilliard equation as follows [20]:

$$\frac{\partial z_X(\mathbf{r},t)}{\partial t} = \nabla \cdot \left[M_X \nabla \left(\frac{\delta G_{\mathrm{sys}}}{\delta z_X(\mathbf{r},t)} \right) \right], \tag{2}$$

where G_{sys} is the total free energy of the system, and M_X is the diffusion mobility of the component *X*. The G_{sys} is defined by

$$G_{\mathrm{sys}} = \int_{\mathbf{r}} \left\{ G_{\mathrm{c}}^{\beta} + \sum_{X=\mathrm{Ti},\ \mathrm{Nb},\ \mathrm{O}} \frac{\kappa_z}{2} (\nabla z_X)^2 \right\} \mathrm{d}\mathbf{r}, \tag{3}$$

where G_{c}^{β} is the Gibbs energy of the β phase and κ_z is the gradient energy coefficient. For simplicity, the values of κ_z for all components are assumed to be identical. Based on the CALPHAD method, the G_{c}^{β} is formulated using the two-sublattice model [18], $(Nb, Ti)_1(O, Va)_3$, where Va denotes the vacancy. The thermodynamic parameters of the phase diagram of the Ti−Nb−O system are used [21-24]. The M_X is related to the impurity diffusion coefficient, D_{Nb} or D_{O} [19,25]:

In this study, one-dimensional simulation was performed for the length scale of 20 nm by using 64 computational grids, and the periodic boundary condition was assumed. The Cahn−Hilliard equation (Eq. (2)) was solved by the conventional finite difference method with explicit Euler technique. In the simulation under the water quenching condition, the temperature was decreased from 1200 K to 300 K with the cooling rate of 500 K s^{-1}. The simulation condition is schematically shown in Fig. 1.

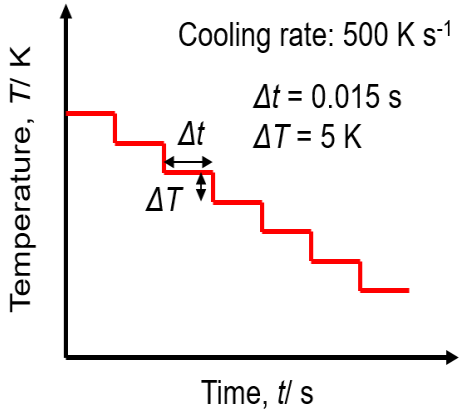

Fig. 1 Schematic representation of the simulation condition of continuous cooling with the rate of 500 K s^{-1}.

3. Results and discussion

The β phase separations in Ti−23Nb−3O (at.%) alloy during isothermal heat treatments are calculated and the results are shown in Fig. 2. Fig. 2a and 2b show the simulation results at 1100 K and 1000 K, respectively. At both temperatures, the β phase separates into Nb-lean β_1 phase and Nb-rich β_2 phase. The composition of the β_1 phase is Nb-lean, Ti-rich and O-rich, while that of the β_2 phase is Nb-rich and O-lean. Using the sublattice model, the β_1 and β_2 phases can be expressed as $(Ti)_1(O, Va)_3$ and $(Nb, Ti)_1(Va)_3$, respectively. The concentration modulation is introduced by the spinodal decomposition in 0.3 ms at 1100 K and in 1.0 ms at 1000 K. The compositional difference between the β_1 and β_2 phases and the wave length of the concentration modulation increase with time. It is seen that the compositional difference between the β_1 and β_2 phases at 1000 K is slightly larger than that at 1100 K, and the spinodal decomposition at 1000 K takes more time than that at 1100 K. The calculation results show that in Ti−23Nb−3O (at.%) alloy, the β phase spinodal decomposition progresses in 0.3−20 ms at 1000−1100 K during the cooling process. When the alloy is water quenched with the cooling rate of 500 K s^{-1}, the decrement of 100 K takes 0.2 s, implying that the spinodal decomposition can occur at 1000−1100 K. The atomic diffusion during water quenching is often ignored but in Ti−Nb−O alloys, it is presumed that the β phase spinodal decomposition occurs even during water quenching.

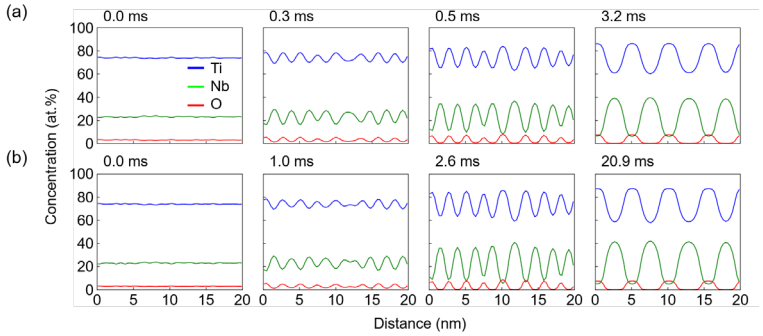

Fig. 2 Simulation results of spinodal decomposition during isothermal heat treatment in Ti−23Nb−3O (at.%) alloy; (a) 1100 K and (b) 1000 K.

In order to investigate the spinodal decomposition behavior during water quenching, the phase-field simulation was performed under the continuous cooling condition with the cooling rate of 500 K s^{-1}. Figure 3 shows the change in the concentration profile during the continuous cooling in Ti−23Nb−1O alloy. The concentrations of all components are homogeneous at 1200 K and 1100 K, and the concentration modulation is observed at temperatures below 1000 K. The β phase spinodal decomposition progresses at 1100−800 K, and the concentration profile at 800−300 K undergoes very little change.

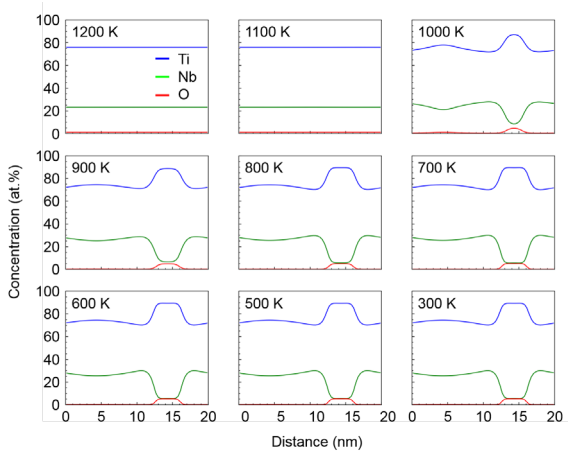

Fig. 3 Simulation result of the change in the concentration profile under the continuous cooling condition with the cooling rate of 500 K s^{-1} in Ti−23Nb−1O alloy.

Figure 4 shows the partial longitudinal section of the metastable phase diagram considering only the β phase in Ti−Nb−O system. In the figure, the Nb composition is fixed to 23at.% and the spinodal line is shown by the dashed line. The temperature of the binodal line increases from about 700 K (Ti−23Nb) to 1150 K (Ti−23Nb−1O) and to

above 1400 K (Ti−23Nb−2O) with increasing O composition, indicating that the addition of a few at.%O to Ti−23Nb alloy induces the β phase decomposition. We see from Fig. 4 that the three-phase region exists at 670−790 K. The calculation results of compositions and fractions of the three β phases in Ti−23Nb−1O alloy are shown in Fig. 5a and 5b, respectively. In this study, Nb-rich phase that appears at temperatures below 750 K is called as β_2' phase. With decreasing temperature, the β_2' phase appears at about 750 K and the β_2 phase disappears at 670 K. Compared to the β_1 phase, both β_2 and β_2' phases are Nb-rich; however, the compositions of the β_2 and β_2' phases are clearly different from each other. The β_2 phase is Ti−Nb-based phase with little oxygen. On the other hand, the β_2' phase is Nb-based phase with little oxygen. Using the sublattice model, the β_1, β_2 and β_2' phases can be expressed as $(Ti)_1(O,Va)_3$, $(Nb, Ti)_1(Va)_3$ and $(Nb)_1(Va)_3$, respectively. The O composition of the β_1 phase in the $\beta_1 + \beta_2$' region is lower than that in the $\beta_1 + \beta_2$ region (see Fig. 5a), and the fraction of the β_1 phase in the $\beta_1 + \beta_2$' region is higher than that in the $\beta_1 + \beta_2$ region (see Fig. 5b). Hence, microstructures that are formed during isothermal heat treatments in the $\beta_1 + \beta_2$ and $\beta_1 + \beta_2$' regions would be quite different from each other.

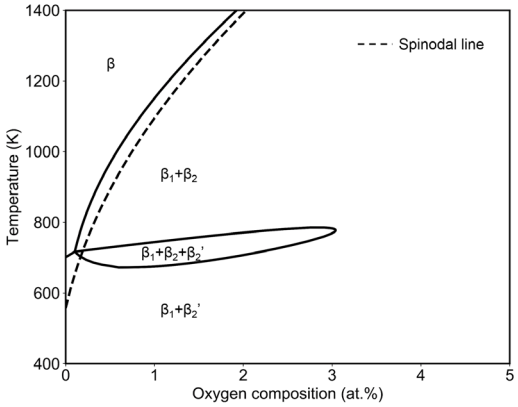

Fig. 4 Calculated partial longitudinal section of the metastable phase diagram considering only the β phase. The Nb composition is fixed to 23at.%.

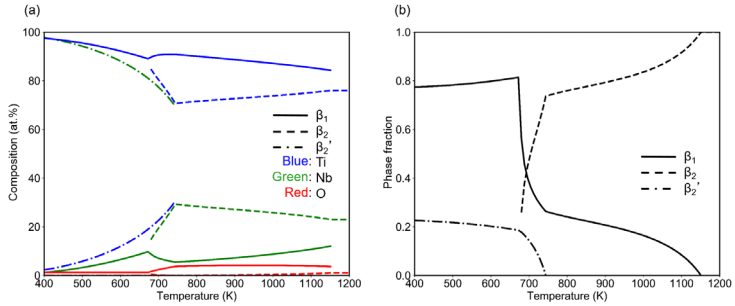

Fig. 5 Calculation results of compositions and fractions of the three β phases in Ti−23Nb−1O alloy; (a) temperature dependence of composition and (b) temperature dependence of phase fraction.

Figure 6 shows the change in the concentration distribution during continuous cooling with the rate of 500 K s^{-1} in Ti−23Nb−1O alloy; the concentration data is extracted from the simulation results shown in Fig. 3. In Fig. 6, the tie line is shown by solid line at each temperature. At 700 K, the alloy composition is inside the three-phase region and hence the three-phase triangle is shown instead of the tie line. In Ti−23Nb−1O alloy, the temperature of the spinodal line is 1090 K. However, we see from Fig. 6 that the spinodal decomposition does not occur at 1050 K during the continuous cooling. The spinodal decomposition progresses at 1050−800 K along the tie lines. As shown in Fig. 5, in Ti−23Nb−1O alloy, there is the $\beta_1 + \beta_2$ phase region at temperatures above 750 K, while the $\beta_1 + \beta_2$' appears at temperatures below 670 K; this is also seen in Fig. 6 because the tie lines at 1050−800 K and 600−400 K are clearly different from each other. The concentration distribution slightly changes at 700−400 K and does not coincide with the tie line of the $\beta_1 + \beta_2$' phase. This result indicates that during the continuous cooling, the concentration modulation introduced by the spinodal decomposition at high temperatures is maintained at low temperatures.

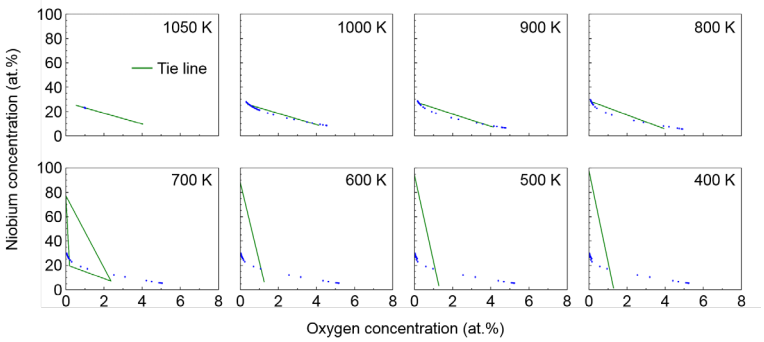

Fig. 6 Change in the concentration distribution during continuous cooling with the rate of 500 K s^{-1} in Ti−23Nb−1O (at.%) alloy. The concentration data is extracted from the simulation results shown in Fig. 3.

The effect of O composition of the alloy on the spinodal decomposition behavior during the continuous cooling was investigated by phase-field simulations. Figure 7 shows the change in the concentration profile during continuous cooling with the rate of 500 K s^{-1} in Ti−23Nb−*X*O alloys (X = 0.6, 1.2, 2.0). The phase decomposition does not occur in Ti−23Nb−0.6O alloy, indicating that there is a critical value of O composition for inducing the spinodal decomposition during water quenching. The concentration

modulation is observed in Ti−23Nb−1.2O alloy at 1100 K, while the spinodal decomposition occurs at 1200 K in Ti−23Nb−2.0O alloy. The spinodal decomposition temperature increases as the O composition increases.

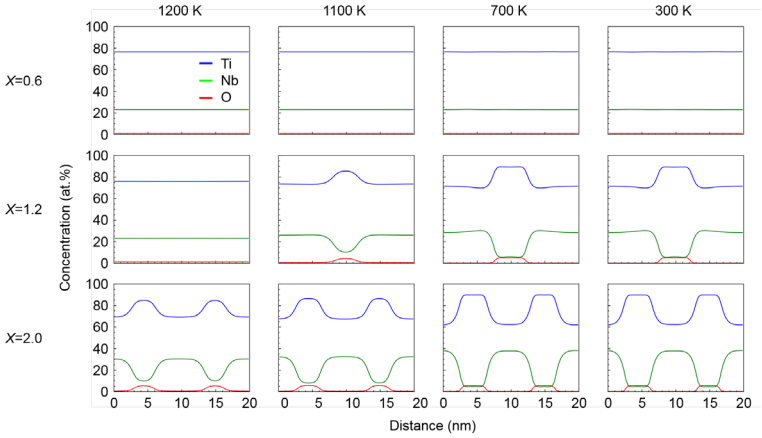

Fig. 7 Change in the concentration profile during continuous cooling with the rate of 500 K s^{-1} in Ti−23Nb−*X*O (at.%) alloys (*X* = 0.6, 1.2, 2.0).

In order to understand the relationship between the β phase spinodal decomposition and the β→α" MT, the driving force of the MT, ΔG_{MT}, corresponding to the concentration profiles at 300 K shown in Figs. 3 and 7 was investigated. The ΔG_{MT} is defined as $\Delta G_{MT} = G_c^{\beta} - G_c^{\alpha"}$; the α" phase is more stable than the β phase when $\Delta G_{MT} > 0$, while the β phase is more stable than the α" phase when $\Delta G_{MT} < 0$. In our calculation, because of the lack of experimental data, the Gibbs energy of the α phase (G_c^{α}) is used instead of $G_c^{\alpha"}$. The concentration profiles of Ti−23Nb−*X*O alloys (*X* = 1.0, 1.2, 2.0) and the corresponding ΔG_{MT} profiles are shown in Fig. 8a and 8b, respectively. In Ti−23Nb−1.0O and Ti−23Nb−1.2O alloys, $\Delta G_{MT} > 0$ in the entire region. However, the β phase stability in the Nb-rich region (β_2 phase) is extremely higher than that in the Nb-lean region (β_1 phase). This is due to the fact that Nb is one of the typical β-stabilizing elements. In Ti−23Nb−2.0O alloy, nanoscale distribution of the α" phase stable region ($\Delta G_{MT} > 0$) and the β phase stable region ($\Delta G_{MT} < 0$) can be seen. Note that ΔG_{MT} is not so influenced by the average composition of the alloy (see dash-dot line in Fig. 8b) but rather is influenced by the degree of the concentration modulation introduced during water quenching. Therefore, careful design of heat treatment and cooling rate conditions is assumed to be necessary to control the β→α" MT behavior and the mechanical properties of Ti−Nb−O alloys.

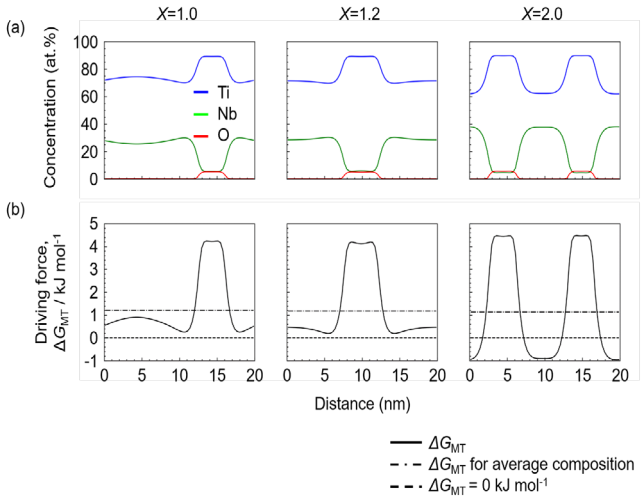

Fig. 8 (a) concentration profiles of Ti−23Nb−*X*O (at.%) alloys (*X* = 1.0, 1.2, 2.0) after the continuous cooling from 1200 K to 300 K with the rate of 500 K s^{-1} and (b) driving force of β→α" martensitic transformation, ΔG_{MT}, corresponding to the concentration profiles shown in (a).

4. Conclusions

The β phase spinodal decomposition during continuous cooling in Ti−Nb−O alloys was investigated by the phase-field method. The obtained results are as follows.

(1) Oxygen addition to the alloy promotes the β phase spinodal decomposition to Nb-rich and Nb-lean phases. In Ti−23Nb−3O (at.%) alloy, the β phase separates into the nanoscale β_1 and β_2 phases that can be expressed as $(Ti)_1(O, Va)_3$ and $(Nb, Ti)_1(Va)_3$, respectively, during isothermal heat treatment at 1100 K and 1000 K. The spinodal decomposition progresses in 0.3−20 ms at 1000−1100 K.

(2) In Ti−23Nb−*X*O alloys (*X* = 0.1−3.0), the three-phase region of the β_1, β_2 and β_2' phases exists at 670−790 K. The β_2' phase can be expressed as $(Nb)_1(Va)_3$. In Ti−23Nb−1O alloy, the tie line of the $\beta_1 + \beta_2$ phase at temperatures above 750 K is clearly different from that of the $\beta_1 + \beta_2$' phase at temperatures below 670 K.

(3) The β phase spinodal decomposition in oxygen-added Ti−23Nb (at.%) alloys occurs during continuous cooling with the rate of 500 K s^{-1}, indicating that the spinodal decomposition progresses during water quenching. The concentration modulation introduced by the $\beta_1 + \beta_2$ spinodal decomposition at 1050−800 K is maintained at lower temperatures during the continuous cooling. The β phase spinodal decomposition has significant effect on the β→α" MT. Hence, careful design of heat treatment and cooling rate conditions is assumed to be necessary to control the mechanical properties of Ti−Nb−O alloys.

5. Acknowledgement

This work was partly supported by the research grant from Kyosho Hatta Foundation.

6. References

[1] M. Niinomi, Metall. Mater. Trans. A 33(3) (2002) 477.

[2] H.Y. Kim, S. Hashimoto, J.I. Kim, *et al*., Mater. Trans. 45(7) (2004) 2443-2448.

[3] H.Y. Kim, Y. Ikehara, J.I. Kim, *et al*., Acta Mater. 54(9) (2006) 2419-2429.

[4] J.I. Kim, H.Y. Kim, H. Hosoda, *et al*., Mater. Trans. 46(4) (2005) 852-857.

[5] Y. Nii, T.-h. Arima, H.Y. Kim, *et al*., Phys. Rev. B 82(21) (2010) 214104.

[6] M. Tahara, H.Y. Kim, T. Inamura, *et al*., Acta Mater. 59(16) (2011) 6208-6218.

[7] M. Tahara, T. Kanaya, H.Y. Kim, *et al*., Acta Mater. 80 (2014) 317-326.

[8] M. Tahara, T. Inamura, H.Y. Kim, *et al*., Scripta Mater. 112 (2016) 15-18.

[9] J.G. Niu, W.T. Geng, Acta Mater. 81 (2014) 194-203.

[10] Y. Ishiguro, Y. Tsukada, T. Koyama, Comput. Mater. Sci. 151 (2018) 222-230.

[11] M. Ikeda, S.-y. Komatsu, Y. Nakamura, MATERIALS TRANSACTIONS 45(4) (2004) 1106-1112.

[12] R. Davis, H.M. Flower, D.R.F. West, Acta Metallurgica 27(6) (1979) 1041-1052.

[13] C.R.M. Afonso, P.L. Ferrandini, A.J. Ramirez, *et al*., Acta Biomater. 6(4) (2010) 1625-1629.

[14] D.L. Moffat, U.R. Kattner, Metall. Trans. A 19(10) (1988) 2389-2397.

[15] H.L. Wang, S.A.A. Shah, Y.L. Hao, *et al*., J. Alloy. Compd. 700 (2017) 155-158.

[16] Y.L. Hao, H.L. Wang, T. Li, *et al*., J. Mater. Sci. Technol. 32(8) (2016) 705-709.

[17] J. Zhu, Y. Gao, D. Wang, *et al*., Acta Mater. 130 (2017) 196-207.

[18] N. Saunders, A.P. Miodownik, CALPHAD : calculation of phase diagrams : a comprehensive guide, Pergamon 1998.

[19] I. Loginova, J. Odqvist, G. Amberg, *et al*., Acta Mater. 51(5) (2003) 1327-1339.

[20] L.-Q. Chen, Ann. Rev. Mater. Res. 32(1) (2002) 113-140.

[21] B.J. Lee, N. Saunders, Z. Metallkd. 88 (1997) 152-161.

[22] R.J. Pérez, A.R. Massih, J. Nucl. Mater. 360(3) (2007) 242-254.

[23] Y. Zhang, H. Liu, Z. Jin, Calphad 25(2) (2001) 305-317.

[24] A.T. Dinsdale, Calphad 15(4) (1991) 317-425.

[25] The Japan Institute of Metals, Kinzoku data book [Metal's data book], third ed. ed., Maruzen, Tokyo, 1993.